Int. J. Heat Mass Transfer. Vol. 34, No. 3, pp. 809–818, 1991
Printed in Great Britain

0017–9310/91 $3.00+0.00

Numerical simulation and field testing of flame-jet thermal spallation drilling—2. Experimental verification

RICK M. RAUENZAHN† and JEFFERSON W. TESTER
Department of Chemical Engineering, Massachusetts Institute of Technology, Cambridge, MA 02139, U.S.A.

(*Received* 7 *June* 1989 *and in final form* 10 *May* 1990)

Abstract—Model predictions are tested against actual measurements of flame-jet induced rock spallation under well-defined experimental conditions. Granites from Barre, Vermont, and Westerly, Rhode Island, are selected for testing. For a small-scale, propane–oxygen supersonic flame-jet, computed heat transfer rates usually matched calibrated values to within 20%, but penetration rates from quarry drilling experiments, another measure of heat transfer effectiveness, are substantially lower than expected by at least a factor of four. Two-phase flow effects and adhesion of rock particulates to the spalling surface, which are not treated rigorously within the model, contribute to this disagreement.

INTRODUCTION

SPALLATION drilling relies on contact between a high-intensity flame-jet and a rock surface to cause flaking of the rock into spalls. Rock failure mechanisms leading to spallation have previously been examined [1, 2], but field operations with a commercial-size torch have not been systematically analyzed prior to the development of our model discussed in Part 1 of this paper. The reliability of actual numerical values and trends in drilling rate and hole radius predicted by our model were tested experimentally by reproducing the combination of these physical processes. Formation of some shallow holes in well-characterized granite at preset penetration speeds using a flame-jet with known utility flows and outlet temperature provided the required data for a reliable check of the computational physics.

Granites from Barre, Vermont, and Westerly, Rhode Island, were selected for testing because they have been characterized extensively [3]. Barre granite is presently actively quarried, and open vertical faces relatively free of imperfections and seams could be readily pierced to produce horizontal holes at known rates. At Westerly, only large boulders were available for spalling tests because the Crumb quarry has been dormant for several years. A scaled-down version of the jet-piercing tools used by Browning [4] and by a Los Alamos team [5] was directed at the block or face of granite and constantly advanced at a predetermined velocity. Unlike the earlier spallation drilling tools, our penetrator used propane and oxygen rather than fuel oil and air. Since the experiments were performed until quasi-steady drilling conditions were attained, knowledge of gas flows and piercing speed, following the computations outlined in Part 1 of this paper, established the desired values of standoff distance and final hole size (and shape). The length of hole required before steady drilling proceeds cannot be estimated from first principles. Thus, the invariance of hole radius after a pierced depth of about 50 cm was the only manner in which to ensure that steady conditions had been reached.

Once several holes had been drilled at different speeds in each granite, the measured hole radius and standoff distance were compared with those predicted from Figs. 3 and 4 of Part 1 of this paper, given the gas flows and penetration rate. One of the goals, then, is to compare experimental and numerical Stanton numbers. Two experimental Stanton numbers can be introduced. The first assumes that heat transfer to a curved wellbore does not depend on the nature of the surface and that the real rock surface is spalling and perturbing the flow by introducing rock chips. In line with this thinking, we performed experiments to calibrate our field torch using a copper block as a calorimeter. Thermocouples were positioned at several key locations within the block to track the transient temperature rise induced by the torch. The other Stanton number assumes that the relationship between heat flux and drilling rate detailed in Part 1 of this paper holds

$$\langle Q \rangle = (\rho C_p)_r V_{dr}(\langle T_s \rangle - T_{r0}) \qquad (1)$$

where $\langle T_s \rangle$ as a function of the average bottom hole heat flux ($\langle Q \rangle$), is given by equation (25) of Part 1. The validity of this relationship and of the simulation results presented in Figs. 3 and 4 of Part 1 will be discussed in relation to the present work and also to Browning's earlier field drilling tests.

The propane–oxygen flame-jet penetrator used in

†Current address: Theoretical Division, Los Alamos National Laboratory, Los Alamos, NM 87545, U.S.A.

NOMENCLATURE

C_p	heat capacity at constant pressure [J kg^{-1} K^{-1}]
$C_{p,\mathrm{jet}}$	heat capacity at constant pressure at jet inlet temperature [J kg^{-1} K^{-1}]
$C_{p,\mathrm{r}}$	rock heat capacity [J kg^{-1} K^{-1}]
C_v	heat capacity at constant volume [J kg^{-1} K^{-1}]
d_t	decline rate of maximum surface heat flux
D	diameter of nozzle [m]
E	Young's modulus [Pa]
h	jet heat transfer coefficient to flat surface [W m^{-2} K^{-1}]
k_{gas}	gas thermal conductivity [W m^{-1} K^{-1}]
m	Weibull homogeneity parameter
p_{jet}	jet pressure at nozzle throat [Pa]
Pr	molecular Prandtl number
Q	heat flux [W m^{-2}]
Q_{exp}	experimentally measured heat flux to copper calorimeter [W m^{-2}]
Q_{max}	maximum or centerline value of heat flux [W m^{-2}]
R_{dr}	radius of flame-jet drill nozzle [m]
R_{h}	hole radius [m]
s	distance from axis along mock wellbore surface [m]
s_0	spreading distance in heat flux distribution [m]
$\langle St\rangle$, $\langle St\rangle_{\mathrm{eff}}$	effective spatially averaged Stanton number
t	time [s]
t_{tot}	total experimental time [s]
T_{jet}	jet temperature [K]
T_{r}	rock temperature [K]
T_{r0}	initial rock temperature [K]
T_{s}	rock surface temperature [K]
$\langle T_{\mathrm{s}}\rangle$	spatially averaged, bottom hole rock spalling temperature [K]
v_{jet}	jet velocity at nozzle throat [m s^{-1}]
V_{dr}	overall rock drilling velocity [m s^{-1}]
Z_{dr}	drilling nozzle standoff distance [m]
Z_{n}	nozzle standoff distance [m].

Greek symbols

α_{r}	rock thermal diffusivity [m^2 s^{-1}]
β_{r}	rock thermal expansion coefficient [K^{-1}]
γ	ratio of gas specific heats, C_p/C_v
μ	Poisson's ratio
ν	gas kinematic viscosity [m^2 s^{-1}]
ρ	density [kg m^{-3}]
ρ_{jet}	gas jet density [kg m^{-3}]
ρ_0	ambient gas density [kg m^{-3}]
ρ_{r}	rock density [kg m^{-3}]
σ_{ob}	overburden stress [Pa].

our experiments resembles a small quarry slotting tool with an o.d. of 3.18 cm (1.25 in.) and a 0.64 cm (0.25 in.) diameter sonic nozzle and is approximately 210 cm (7 ft.) in overall length. However, the combustion gases from most conventional quarry slot-cutting tools that use fuel oil in oxygen are directed away from the centerline of the burner housing at the exit. Therefore, because the combustion products from our propane–oxygen torch must exit symmetrically along the jet tool axis, the configuration of our apparatus was not identical to those that are commercially available. Inlet fittings were compatible with standard gas hose couplings (nominally 1/4 in.), and an inlet and an outlet connection for cooling water were also provided.

The scaled-down penetrator was mounted on a rack constructed with vertical and horizontal angle steel crossbars and a sheet of plywood that served as the base for the penetrator assembly. The plywood supported a variable speed gear motor (single phase, 120 V, 187 W (1/4 hp), top speed 1750 rev min^{-1}) with a 10 : 1 speed reducer gear box on the drive shaft. Through a Lovejoy flexible coupling, a 2.22 cm (7/8 in.) threaded rod was driven by the motor and acted as the advancing mechanism for the jet tool. The distant end of the rod passed through a bearing plate, also 2.22 cm, to lend support to the rod while allowing unrestricted rotation. Two 2.22 cm threaded pipe couplings welded to 3.18 cm pipe hangers travelled linearly on the threaded rod at a forward (or backward) speed determined by the rotation speed of the motor and the nine threads per inch on the rod. Thus, the advance speed of the drill, once set in the pipe hangers and firmly attached, could be determined to within 5% by monitoring the number of seconds elapsed during nine revolutions of the drive shaft and Lovejoy coupling.

At Barre, open quarry faces, perhaps 10–50 m deep, of bare granite occur regularly at points within the quarry where rock is unsuitable for production. However, seams and other defects that prohibit commercial use of this rock section were sparse enough that holes several feet deep could be pierced in relatively uniform granite. In the Crumb quarry at Westerly, Rhode Island, the only easily accessible granite was present in the form of large boulders on the edge of the quarry wall. In the procedure for an experimental run, the rack and drill assembly was positioned directly in front of the granite face in Barre or on top of it in Westerly. The burner nozzle was initially held about 10–15 cm from the rock surface. After ensuring that a reasonable cooling water flow of at least 1.1 m^3 h^{-1} (5 gpm) had been established, the torch was ignited. Then, the motor was started, and

the penetrator was advanced toward the rock at the desired rate.

After approximately 50 cm of drilling, the motor was shut off, and the propane and oxygen flows were quickly terminated to halt spallation. The standoff distance was determined with a metal measure. The variation of hole radius as a function of depth was also examined visually to determine whether steady drilling conditions had been achieved. If the hole radius was invariant over approximately one-third to one-half of the total depth, then steady state was assumed to exist near the end of the experimental test. The hole diameters produced ranged from 7.5 to 15 cm and diameter variations with hole depth near the end of the hole were observed to be small. Therefore, steady-state conditions presumably prevailed during the final stages of each run.

Often, particularly at the Barre test site, large chunks of glowing, partially melted rock would suddenly spew from the hole, probably after being trapped in the annular space between drill and hole. This behavior has not been reported previously, though observation of such large rock conglomerates would not be expected from a deeper hole, because more time for disintegration of the mass into individual particles is available as it travels up the well. Furthermore, the greater annular spacing between drill housing and hole in larger drilling systems would not impede the exhausting of spalled rock.

The most probable mechanism for generation of these partially melted masses is caused by near-surface imperfections inherent in the rock. If the relatively massive portion of granite affected by heat to the point of thermal failure along the pre-existing seam enters the hole, its rapid removal is not guaranteed. The introduction of rock chunks into the hole, while greatly complicating gas and particle flow during the experiment, is not typically expected in deep basement rock, far from any weathered regions.

Despite the difficulties encountered during completion of the experiments, the reproducibility and consistency of trends in the results given in Table 1 indicate that the effects of these complications were not too severe. Drilling velocities ranged from 2.7 to 7.3 m h^{-1}, creating holes between 7 and 17.8 cm in diameter with resulting standoff distances between 6.4 and 21.6 cm. For comparison, non-dimensionalized hole radii and standoff distances are tabulated, as well. Moreover, assuming equation (1) is valid, then equation (1) and equation (25) of Part 1 provide two equations that can be solved for the two unknowns $\langle Q \rangle$ and $\langle T_s \rangle$, known V_{dr} from experiments. Under these conditions, an approximate value of the effective Stanton number can also be obtained to compare with the results given in Fig. 3 of Part 1

$$\langle St \rangle_{eff} \equiv \frac{\langle Q \rangle}{(\rho C_p v)_{jet}(T_{jet} - \langle T_s \rangle)} = \frac{(\rho C_p)_r V_{dr}(\langle T_s \rangle - T_{r0})}{(\rho C_p v)_{jet}(T_{jet} - \langle T_s \rangle)}. \quad (2)$$

An alternative method of determining $\langle St \rangle_{eff}$ not relying on the validity of equation (1) requires a heat flux calibration of the supersonic torch, experimentally determining $\langle Q \rangle$ through calorimetry tests. In this case, therefore, an independent check of the validity of the heat balance at the rock–fluid interface (equation (1)) was generated while obtaining values of the surface heat flux for several standoff distances.

HEAT FLUX CALIBRATION OF SUPERSONIC TORCH

To compare the effective Stanton numbers expected from the numerical model with those achieved during experimental drilling runs, the heat transfer characteristics of jet impingement on the concave cavity formed by the advancing wellbore were examined. A copper block used for previous calibration experiments [1, 6] was first machined into a disk 38.1 cm in diameter. Then the disk was reworked to replicate the hole geometry by milling an ellipsoidal cavity of revolution with major and minor diameters of 15 and 7.5 cm such that the major axis coincided with the disk centerline. Although the exact shape of the bottom hole region in spalling rock will depend somewhat on the actual conditions of the gas jet and drill penetration speed, this single calibration apparatus should experience values of the overall heat transfer rate comparable to those expected with other similar configurations.

Thermocouples were then positioned in wells drilled into the back face of the copper disk at key points within the calorimeter. High conductivity graphite grease enhanced thermal contact between the ten type K thermocouples and the copper in the thermocouple well. The reference junction box, Hewlett–Packard voltmeter, scanner, and desk-top computer were all identical to previous calibration experiments [1, 6]. Insulation on unheated surfaces was supplied by alumina refractory bricks and fiberglass building insulation on the curved and flat faces of the copper, leaving only the 'hole' exposed to heat. To commence a transient calibration, the torch was mounted in ring stands at the desired nozzle-bottom hole standoff. After the copper surface was polished and cleaned, cooling water flow was begun, the scanner was activated, and the torch was ignited (see ref. [6] for details). After 2 or 3 min, the torch was extinguished quickly and the block allowed to cool before attempting another test.

Typically, the thermal rise monitored by all thermocouples in all experiments can be characterized by a fairly sharp rise in temperature followed by an extended, often almost linear increase in time. Given the shape of the response curves, the process of deconvoluting the actual heat flux delivered was expected to be fairly straightforward. However, data regarding the correct spatial form of the heat flux distribution induced by supersonic jets on concave targets have not been reported in the literature. Therefore, the

Table 1. Results of quarry drilling experiments

Drilling velocity, V_{dr} ($m\,h^{-1}$)	Standoff distance, Z_{dr} (cm)	Hole radius R_h (cm)	$\frac{Z_{dr}}{R_{dr}}$	$\frac{R_h}{R_{dr}}$	$\langle St \rangle$
		Barre			
2.74	21.6	8.9	70	28	4.4×10^{-4}
3.25	12.0	7.6	42	24	5.3
4.11	10.2	6.4–7.0	34	20–22	7.1
4.57	10.2	5.7–6.4	34	18–20	8.0
5.49	7.6	3.8–4.4	26	12–14	9.9
6.31	7.6	3.8	26	12	1.2×10^{-3}
6.77	6.4	3.2–3.5	22	10–11	1.3
7.31	7.0	3.5	24	11–12	1.4
		Westerly			
3.39	17.1	7.6–8.3	56	24–26	3.8×10^{-4}
4.57	15.2	6.4–7.0	50	20–22	5.4
5.62	10.2	5.7–6.4	34	18–20	6.9
6.31	8.9	4.4–5.1	30	14–16	7.9

Properties used in evaluating $\langle St \rangle$†

		Barre	Westerly
$(\rho C_p)_r$	($J\,m^{-3}\,K^{-1}$)	2.64×10^6	2.64×10^6
α_r	($m^2\,s^{-1}$)	1×10^{-6}	1×10^{-6}
E	(GPa)	45	50
β_r	(K^{-1})	8×10^{-6}	1×10^{-5}
σ_0	(MPa-$m^{3/20}$)	70	70
m		20	20

Gas properties and flows

$T_{jet} = 2830$ K
$C_{p,jet} = 1880$ J $kg^{-1}\,K^{-1}$
$p_{jet} = 0.45$ MPa
$\gamma = 1.26$
Oxygen flow $\simeq 0.3$ $m^3\,min^{-1}$ STP
Propane flow (by stoichiometry) $\simeq 0.06$ $m^3\,min^{-1}$ STP

† $\langle St \rangle = \dfrac{(\rho C_p)_r(\langle T_s \rangle - T_{r0})}{(\rho C_p v)_{jet}(T_{jet} - \langle T_s \rangle)}$.

form of the heat flux as a function of arc length along the surface was postulated in this study.

The finite-element conduction code, AYER, written at Los Alamos National Laboratory [7], was used to numerically reproduce the transient temperature rise in the copper for these calibrations. The mesh constructed for the analysis of these calorimeter experiments approximated the curvature of the mock wellbore through piecewise linear segments, while conforming to the straight-edged walls and faces of the copper block. Insulated faces of the copper block were modeled as zero heat flux boundaries. Thus, only the ellipsoidal, heated surface was modeled in detail.

It is tempting, given the excellent fits obtained in earlier calibration tests [1, 6], to consider a simple modification of Anderson and Stresino's [8] heat flux distribution for jet impingement on a flat surface, given in the following form:

$$Q(s) = Q_{max} \exp(-s/s_0) \tag{3}$$

where, in this case, s denotes the distance along the curved face as tracked from the centerline of the disk (also the axis of the ellipsoid), not the radial distance from the axis of symmetry. This assumption is consistent with the compiled experimental evidence of Hrycak [9], which supports the remarkable similarity among boundary layer wall-jet flows resulting from impingement on flat, convex, and concave objects.

However, attempts to numerically match the data, using the identical search routine proposed by Nelder and Mead [10], were not as successful as previous parameter searches would have indicated. For instance, the deviation between computation and experiment continues to grow as time passes, unlike previous calibration fits for a flat copper disk heated by a subsonic propane torch [1, 6]. Apparently, although nominally straight-line sections of temperature vs time histories existed for flat plate experiments, the postulated form of the heat flux distribution on the curved surface consistently overestimates the rate of temperature increase at late times. All thermocouple positions exhibited this anomaly. Other empirical forms of $Q(s)$, the heat flux distribution, including uniform and exponential functions

$$Q(s) = Q_{max}, \quad s < s_0$$

$$Q(s) = Q_{max} s^n \exp(-s/s_0), \quad s > s_0, \quad n = 1,2 \quad (4)$$

did not improve the fit.

Conceivably, $Q(s)$ could be exhibiting some time dependence because of the consistent increase in disagreement between experimental thermocouple temperatures and numerical fits. In an effort to match this, a time correction was superimposed on the heat flux distribution of equation (3)

$$Q(s) = Q_{max}(1 - d_t(t/t_{tot})) \exp(-s/s_0) \quad (5)$$

to allow a linear decay of the heating rate over the term of the experiment (t_{tot}). From the three-parameter (Q_{max}, s_0, d_t) search routine, the optimal values produced were able to follow the experimental data more satisfactorily, but not as well as the original Anderson and Stresino form (equation (3)) did in the flat-disk calibration. Several potential causes for this time-dependency were examined in detail. These included (1) thermocouple conduction away from the contact surface, (2) excessive heat losses through the insulation, (3) decrease in the temperature difference between the flame and the copper surface during the course of the experiment, violating the constant heat flux assumption, and (4) a progressively decreasing propane supply during the course of the experiment on cooler days. No single effect could fully explain the apparent observed decline in jet heat transfer rate. In future tests, careful attention must be devoted to thermal contact between thermocouples and the calibration material. Also, if cooler days are chosen for experimental tests, a constant flow of propane should be maintained by supplying external heating to the reserve tank and supply lines.

The final heat transfer correlations (Table 2) for maximum heating rate (Q_{max}) are relatively invariant with standoff distance. Generally, the available literature data for subsonic jets are not consistent with these experimental results if Z_n/D exceeds about 8. For example, Kataoka *et al.* [11] proposed a substantial dependence on relative standoff distance (Z_n/D)

$$\frac{hD}{k_{gas}} = 8.5\left(\frac{\rho_{jet}}{\rho_0}\right)^{0.5}\left(\frac{D}{Z_n}\right)^{0.88}\left(\frac{v_{jet}D}{\nu}\right)^{0.5}(Pr)^{0.5}. \quad (6)$$

Table 2. Results of heat flux calibration experiments

Standoff distance (cm)	Q_{max} (MW m^{-2})	s_0 (cm)	d_t	Estimated range of Q_{max} (MW m^{-2})
7.6	5.6	5.1	0.05	5.3–5.6
7.6	7.1	4.0	0.32	4.8–7.1
10.2	5.3	5.2	0.21	4.2–5.3
10.2	7.4	3.0	0.38	4.6–7.4
10.2	5.4	4.8	0.15	4.6–5.4
12.7	5.3	3.0	0.48	2.8–5.3
15.2	5.4	3.7	0.43	3.1–5.4

Oxygen flow $\simeq$ 0.3 m^3 min^{-1} STP.
Propane flow (by stoichiometry) $\simeq$ 0.06 m^3 min^{-1} STP.

However, as Piesik and Roberts [12] demonstrated, the equivalent 'potential' core length for most supersonic jets often extends to at least 20 nozzle diameters. Thus, the fairly constant heating rate can be partially attributed to the structure of supersonic impinging jets. For Z_n/D higher than about 20, the heat transfer coefficient should decline rapidly as subsonic jet behavior dominates the downstream flow. The only calibration performed at larger spacings did not exhibit markedly different results, but more experiments are necessary before definite conclusions can be drawn.

Including the time variation of heat flux, the heat transfer rate is somewhere between 3 and 7 MW m^{-2}. The actual flux present during field drilling tests was probably somewhere within the relatively wide range of measured maximum and minimum values. As will be demonstrated, some useful inferences can be extracted from comparison of experimental and numerical effective Stanton numbers, despite the somewhat questionable quality of the numerically estimated heat fluxes to the copper calorimeter.

COMPARISON OF DRILLING EXPERIMENTS WITH NUMERICAL PREDICTIONS

The most convenient method of comparing the results of small-scale quarry tests with the numerical simulations is to compare both effective Stanton numbers and non-dimensional hole radii. As shown in Fig. 1, agreement in trends and actual values between predicted numerical and experimental hole radii is extremely close. The predicted diameter, especially as standoff increases, tends to slightly underestimate the

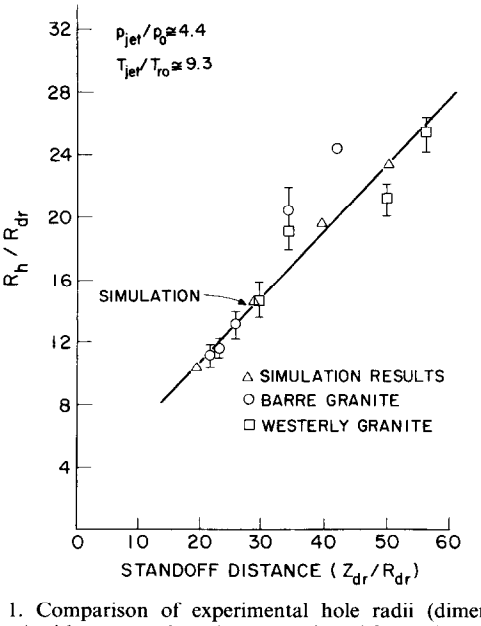

FIG. 1. Comparison of experimental hole radii (dimensionless) with computed results, cross-plotted from Fig. 4 of Part 1.

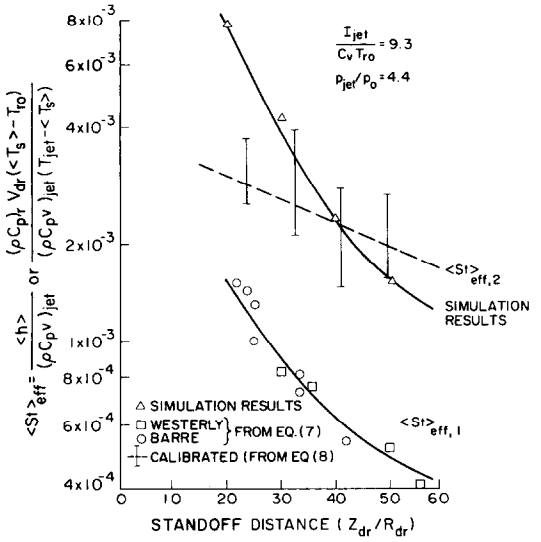

FIG. 2. Comparison of Stanton numbers deduced from experimental penetration rates ($\langle St\rangle_{eff,1}$) and those from copper calibrations ($\langle St\rangle_{eff,2}$) with computed results, cross-plotted from Fig. 3 of Part 1.

actual drilled hole size, but the scatter in the experimental data encompasses code-generated results.

Figure 2 shows that disagreement between experimental and numerical heat transfer rates cross-plotted from Fig. 3 of Part 1 depends strongly on the method of calculating the Stanton numbers ($\langle St\rangle_{eff}$). For constant jet velocities and temperatures, the magnitude of $\langle St\rangle_{eff}$ is controlled by the value for surface heat flux. Therefore, for drilling experiments, two distinct Stanton numbers are possible: one relying on the integral heat balance at the rock surface (equation (1))

$$\langle St\rangle_{eff,1} \equiv \frac{(\rho C_p)_r V_{dr}(\langle T_s\rangle - T_{ro})}{(\rho C_p v)_{jet}(T_{jet} - \langle T_s\rangle)} \tag{7}$$

where $\langle T_s\rangle$ is calculated from simultaneous solution of equation (1) and equation (25) of Part 1 of this paper. The other uses the calibrated heat flux (Q_{exp}) from the copper block

$$\langle St\rangle_{eff,2} \equiv \frac{Q_{exp}}{(\rho C_p v)_{jet}(T_{jet} - \langle T_s\rangle)} \tag{8}$$

where $\langle T_s\rangle$ is calculated from equation (25) of Part 1. If equation (8) is used, thereby not relying on equation (1), then the Stanton numbers match well, except for the dependence of experimental $\langle St\rangle_{eff,2}$ at low standoff distances. If heat flux is obtained from the integral heat balance (equation (1)), then the discrepancy between computed and experimental Stanton numbers grows to a factor of four. Apparently, the accuracy of relating the heat supplied with rock drilling speed in such a simple fashion (equation (1)) must be questioned. Using equation (8) for $\langle St\rangle_{eff}$ also contains an implicit assumption that the two heat transfer processes, those between the flame-jet and the spalling granite and from the flame-jet to the copper, are not radically different. The validity of these assumptions will now be examined.

If the heat balance (equation (1)) is valid, then the considerable difference between numerical and experimental values must be reconciled. The most compelling argument for relying solely on the heat balance relationship is the remarkable agreement in trend (but not magnitude) of the numerical and quarry drilling results. In addition to numerical uncertainties inherent in the calculations, several physical causes were examined.

The first involves any heat losses from the system (not accounted for in the numerical simulations). For instance, any heat conducted to the hole bottom will clearly be eventually regained in the form of spalls. Therefore, the maximum amount of heat that could be wasted is conducted away from the nearly vertical surface of the included cylindrical wellbore. Using Goldenberg's [13] solution for heat conducted through the faces of a uniformly heated, stationary cylinder, an upper bound on the amount of heat loss can be obtained for drilling. With his model heat losses are estimated to be insignificant if drilling is extended over a period 1 h or longer. During the time scale of the quarry tests (10–15 min) and at drilling rates (V_{dr}) of 0.002 m s^{-1}, heat conducted and lost to the surroundings can be almost 25% of the heat returned by rock spalls. However, this is still only a small fraction of the factor of three or four between numerical trends and the experimental curve derived by applying the heat balance (equation (1)).

Another reason to doubt the validity of the heat balance as employed here lies in the accuracy of the

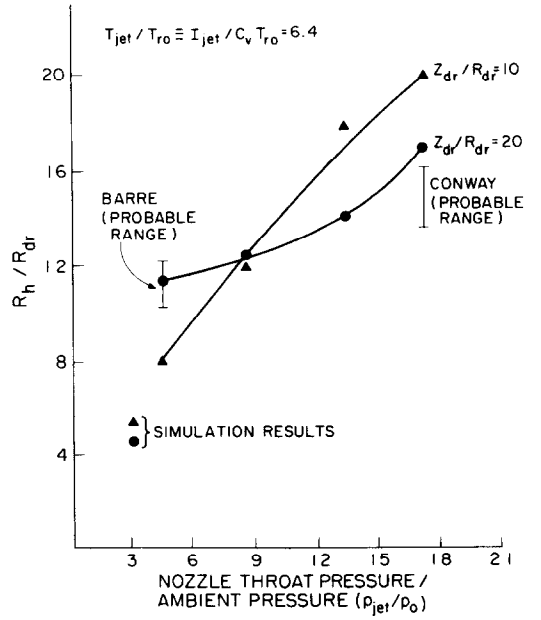

FIG. 3. Comparison of Browning's experimental hole radii (dimensionless) with computed results, for two different operating pressures in nozzle throat (cf. Table 3).

spallation temperature relationship. Until now, the extension of Weibull statistics proposed by Dey [2] was used to determine the surface temperature at spallation (equation (25) of Part 1). The measurements of ΔT_s performed in ref. [1], especially those from propane torch-induced spallation, agreed well with the theoretical values. However, only onset of spallation was considered, which typically occurred when $(T_s - T_{r0})$ approached 400–450 K. If, for instance, continued penetration requires a surface temperature rise of 1000 K, then $\langle St \rangle_{eff,1}$ would be adjusted upward by a factor of over two. Also, as noted by Soles and Geller [14], many other processes, such as quartz phase transition and dolomite decomposition, potentially initiate at these elevated temperatures. No physical evidence for these mechanisms has ever been reported during Canadian Mines Bureau studies [14, 15] or Union Carbide-sponsored research of spalling mechanics [16]. The only reasonable manner of resolving the issue of true spallation temperature during drilling will require direct radiative measurement of surface conditions.

The assumptions inherent in numerical computations and the potential difference in heat transfer mechanisms between flame-jets and copper or granite surfaces were also examined. If the heat fluxes to copper actually overestimated those expected to a spalling rock surface, then equation (8) would not supply the correct Stanton number value under drilling conditions. Heat transfer to roughened granite surfaces computed by the simulation agrees well with that deduced from copper calibration tests, and the numerical model might be neglecting an important physical process that effectively impedes heat transfer to spalling rock. Full account for the effects of the solid phase of chips in the flow field could drastically alter present results. No consideration of turbulent interactions between spalls and hot fluid is incorporated into our model (see Part 1).

The physical condition of the rock surface is also of primary importance. Apart from assessment of surface temperature, the effective heat transfer coefficient to the spalling surface will depend strongly on stagnant regions of fluid trapped by partially adhered spalls. During the Barre granite drilling tests, a substantial retardation of chip removal can be attributed to the 'glue-like' nature of fused biotite impeding complete separation of the spall from the underlying rock. The overall heat transfer coefficient produced by flowing gas will decrease due to added heat flow resistance caused by conduction through semi-stagnant fluid trapped under the spall.

In short, apart from numerical inaccuracies that were mentioned in the conclusions to Part 1 of this paper, the discrepancies between numerical and experimental drilling rates cannot be explained completely by any single physical process occurring during the experimental tests. Rock chips adhering to the surface and effects of spalls on fluid turbulence intensity remain the most likely explanations for the disagreement.

COMPARISON OF NUMERICAL RESULTS WITH OTHER FIELD INVESTIGATIONS

Comparisons with other existing field data are more difficult, primarily due to lack of key operating information. Although drill standoff distance would not be of concern to field operators, its value is crucial in establishing heat flux to rock near the hole bottom. In fact, no other investigator has ever reported a steady-state drill standoff, since, in practice, penetration speed is of utmost priority. Moreover, Browning [4] is the only researcher who has pierced rock to any extent with a single-nozzle flame-jet, but his operations in the Conway and Barre granite quarries probably never reached steady conditions. Thus, matching numerical results with his experiments is not a definitive test of the code's reliability. If instantaneous penetration rates and hole diameters are averaged over the course of drilling and plotted with the simulation results, now as a function of pressure at a set temperature (Figs. 3 and 4), then the general level of agreement between the code and a real, fairly extensive drilling program can be determined. The relevant physical properties used in determining $\langle Q \rangle$ and $\langle T_s \rangle$ for Browning's work are presented in Table 3.

Again, although the code produces a satisfactory estimate of hole radius, it significantly overestimates the actual drilling rate, particularly in the drilling of the shallower hole at Barre, Vermont, that used a lower pressure of combustion air. Although standoff distance is unknown, Browning's experience in drilling holes has guided him in sensing the standoff distance that he believes leads to optimal penetration rate. Therefore, the worst-case comparison between

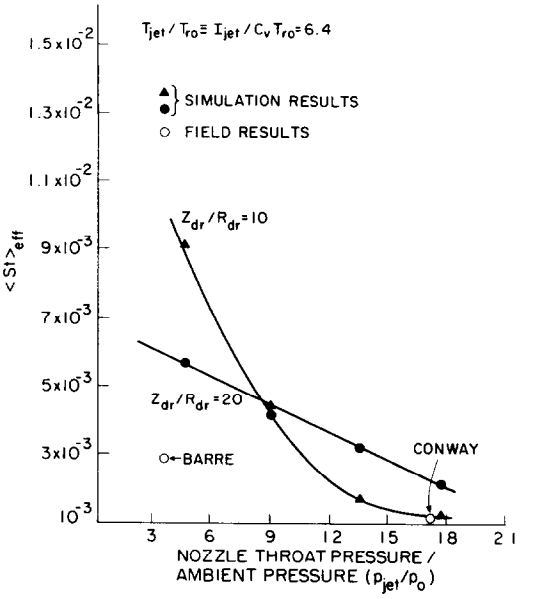

FIG. 4. Comparison of Browning's experimental drilling rates (restated in terms of Stanton number) with computed results, for two different operating pressures in nozzle throat (cf. Table 3).

Table 3. Physical properties and operating parameters for Browning's drilling exercises in Conway and Barre

		Barre	Conway
Rock properties			
$(\rho C_p)_r$	(J m^{-3} K^{-1})	2.64×10^6	2.64×10^6
α_r	(m^2 s^{-1})	1×10^{-6}	1×10^{-6}
E	(GPa)	45	50
β_r	(K^{-1})	8×10^{-6}	1×10^{-5}
Weibull parameters			
σ_0	(MPa-m$^{3/20}$)	70	70
m		20	20
Hole characteristics			
V_{dr}	(m h^{-1})	7.6	16–30(?)
R_h	(m)	0.38–0.45	0.25 0.30
Gas properties (calculated at nozzle throat)			
$(\rho C_p)_{jet}$	(J m^{-3} K^{-1})	1170	4510
T_{jet}	(K)	1940	1940
R_{dr}	(cm)	3.81	1.91
p_{jet}	(MPa)	0.46	1.75
$\gamma = C_p/C_r$		1.26	1.26

results would use a predicted average heat transfer at low pressure ($p_{jet}/p_0 = 4.4$) somewhat in excess of that expected at $Z_{dr}/R_{dr} = 10$, since the 'optimal' standoff distance, if one exists, is expected to be less than 10. Likewise, at the elevated pressures ($p_{jet}/p_0 = 17.5$) at which Browning's torch operated in Conway, the predicted optimal standoff distance is probably near 20. Generally, numerical and actual heat transfer predictions disagree by about a factor of 3–4, as in the smaller-scale quarry piercing runs.

Here, however, the instantaneous penetration rate data gathered and reported by Browning as a function of total hole depth point to another possible source of error, aside from those discussed above (unusually high heat losses to the surrounding earth, higher actual T_s than expected, numerical errors, partially adhering chips, and two-phase flow effects). As the Conway hole neared completion, after about 320 m depth, the drilling rate began to climb steadily until operations ceased at about 340 m. Browning attributed this increase in speed to accumulation of earth stresses with depth. However, an estimated bound on the additional stresses (σ_h) induced by excavating a cavity can be obtained by assuming that the earth behaves in a linearly elastic fashion [17]

$$\sigma_h = \sigma_{ob} \frac{3\mu}{1-\mu} \tag{9}$$

where σ_{ob} represents the overburden stress, or that generated by the weight of rock over a depth h. For $\mu = 0.25$ and $\rho_r = 2600$ kg m^{-3}, the additional stresses are, at most, 10 MPa, well below the nominal compressive strength of granite of about 200 MPa. A more attractive and defendable explanation would suggest that at the total eventual depth (or near it), Browning began to pierce undamaged, unweathered rock without any water-bearing zones for the first time. In fact, his drilling log of the entire operation cites many instances where seams, fractured rock, and water inflow momentarily impeded drilling progress. Because numerical computations have no mechanism for including similar discontinuities in rock structure, perhaps the appropriate value of V_{dr} should be 30 m h^{-1}, that attained at the end of drilling, as opposed to the average, which is about half of that. The Barre hole, not as deep (140 m), might not have extended beyond the damaged region, and the potential maximum steady-state drilling rate of the system was presumably not reached.

During our quarry drilling tests at Barre, some large chunks of broken rock periodically fell from the sidewalls into the hole. The cliff used for these experiments was naturally fractured and exhibited major seams every 1–2 m near the portion of the face used. One possible major cause of the unexpectedly low drilling rates is that all drilling in these quarry tests, indeed nearly all field tests of spallation drilling completed to date, has been attempted in rock containing gross imperfections. Presumably, in deep drilling applications, rock competency should progressively improve, yielding behavior closer to the 'true' drilling characteristics of the system. In the future, if possible, drilling of this sort should be performed in the most competent, defect-free mass of rock available to avoid complications introduced by spalling in or near seams and gross fractures.

CONCLUSIONS

Complications that appeared in attempting to form some well-defined holes under controlled conditions and calibrating heat flux from the torch hindered efficient testing of the numerical simulation. Possible interference from inherent rock structural imperfections, variability of propane flow, and frequent clogging of the hole by chunks of partially molten rock confounded efforts to gather reliable data. The consistency among the experimental results, even between two granites with somewhat dissimilar spalling characteristics, points to the quality of the data, however, and most of the discrepancies between experimental and computed heat transfer rates probably result from assumptions made during simulation development (see Part 1).

Heat losses to the earth throughout the duration of the experiment can realistically be, at most, 25% of the total thermal energy delivered to the rock. The absence of phase transitions or mineral melting reported by other investigators [14, 15] and indirect measurements performed in this research [1, 6] would indicate that spallation is a relatively low-temperature (< 700°C) process. Therefore, a factor of three to four disagreement remains unexplained. Nonetheless, the calibrated heat fluxes, despite their uncertainties, agree extremely well with computed values.

Though possessing many simplifications and first-order approximations, our simulation presented in

Part 1 reliably predicts the correct range of heat transfer for a supersonic jet impinging on a curved, concave body, as confirmed by calibration. Therefore, the most plausible computational sources of difficulty are found in two physical processes inherent to spallation that the numerics have not completely addressed and which would not be a factor during any torch calibrations: (1) adhesion of chips to the surface, thereby impeding subsequent gas–rock heat transfer, and (2) disruption of the flow field by solid-phase effects. Although momentum transfer between the time-averaged chip and gas flow fields and surface roughness have been included computationally, the complex turbulent interactions have made it impossible to rigorously account for all expected heat transfer modifications by the two-phase flow. Inclusion of these two-field flow dynamics and higher accuracy finite-difference techniques are the next model improvements that should be undertaken and are presently being considered.

Acknowledgements—The authors wish to thank Robert M. Potter, Hugh Murphy, and Bert Dennis of Los Alamos National Laboratory, which provided partial funding of this work, for their useful advice and the use of equipment. James Browning provided the knowledge he had gained in years of spallation drilling experience. The Rock of Ages Corporation of Barre, Vermont, allowed us to use their quarry faces. In particular, we would like to acknowledge Jerry Parrott, Jon Gregory, and Dorothy Richter of Rock of Ages for their efforts.

REFERENCES

1. R. M. Rauenzahn and J. W. Tester, Rock failure mechanisms of flame-jet thermal spallation drilling: theory and experimental testing, *Int. J. Rock Mech. Geomech. Abstr.* **26,** 381–399 (1989).
2. T. N. Dey, More on spallation theory, Los Alamos National Laboratory Internal Memorandum No. ESS-3-286-84 (1984).
3. R. D. Lama, *Handbook on Mechanical Properties of Rocks*. Trans. Tech., Clausthal, F.R.G. (1978).
4. J. A. Browning, Flame-jet drilling in Conway, NH, granite, unpublished report of work done under University of California order number 4-L10-2889R-1 for Los Alamos National Laboratory (1981).
5. R. E. Williams, Thermal spallation drilling, 9th Conf. Geotherm. Res. Coun., Los Alamos National Laboratory Report LACP-85-20, pp. 69–73 (1985).
6. R. M. Rauenzahn, Analysis of rock mechanics and gas dynamics of flame-jet thermal spallation drilling, Ph.D. Thesis, Mass. Inst. of Technol. (1986).
7. R. G. Lawton, The AYER heat conduction computer program, Los Alamos Scientific Laboratory Report LA-5613-MS (1974).
8. J. E. Anderson and E. F. Stresino, Heat transfer from flames impinging on flat and cylindrical surfaces, *Trans. ASME*, Series C, *J. Heat Transfer* **85,** 49–54 (1963).
9. P. Hrycak, Heat transfer from a row of impinging jets to concave cylindrical surfaces, *Int. J. Heat Mass Transfer* **24,** 407–419 (1981).
10. J. A. Nelder and R. Mead, A simplex method for function minimization, *Computer J.* **7,** 308–313 (1964).
11. K. Kataoka, H. Shundoh, H. Matsuo and Y. Kawachi, Characteristics of convective heat transfer in non-isothermal, variable-density impinging jets, *Chem. Engng Commun.* **34,** 267–275 (1985).
12. E. T. Piesik and D. J. Roberts, A method to define low-altitude rocket exhaust—characteristics and impingement effects, *J. Spacecraft* **7,** 446–451 (1970).
13. H. Goldenberg, Some numerical evaluations of heat flow in the region bounded internally by a circular cylinder, *Proc. Phys. Soc.*, Series B 256–260 (1956).
14. J. A. Soles and L. B. Geller, Experimental studies relating mineralogical and petrographic features to the thermal piercing of rocks, *Tech. Bull. Mines Branch Can.* TB 53 (1964).
15. L. B. Geller, A new look at thermal rock fracturing, *Trans. Inst. Min. Metall.* **79,** A133–A170 (1970).
16. D. C. Freeman, Jr., J. A. Sawdye and F. A. Mumpton, The mechanism of thermal spalling in rocks, *Colo. Sch. Mines Q.* **58,** 225–252 (1963).
17. J. C. Jaeger and N. G. W. Cook, *Fundamentals of Rock Mechanics*. Chapman & Hall, London (1979).

SIMULATION NUMERIQUE ET ESSAIS DU PERCAGE PAR DELITEMENT THERMIQUE A L'AIDE D'UN JET DE FLAMME—2. VERIFICATION EXPERIMENTALE

Résumé—Les prévisions du modèle sont testées par des mesures sur un cas réel de délitement par jet de flamme dans des conditions expérimentales bien définies. On a sélectionne des granits en provenance de Barre, Vermont, et Westerly, Rhode Island. Pour un jet de flamme supersonique propane–oxygène, les flux thermiques calculés sont vérifiés à mieux que 20% près, mais les vitesses de pénétration qui constituent une mesure de l'efficacité du transfert thermique sont nettement inférieures à celles calculées, dans un rapport de quatre. Ce désaccord est à relier aux effets de l'écoulement diphasique et à l'adhésion des particules de roche sur la surface, ce qui n'est pas considéré dans le modèle.

NUMERISCHE SIMULATION UND ERPROBUNG EINES BOHRVERFAHRENS AUF DER GRUNDLAGE DES TEMPERATURBEDINGTEN ABPLATZENS VON MATERIALIEN IN EINEM FLAMMSTRAHL—2. EXPERIMENTELLE BESTÄTIGUNG

Zusammenfassung—Modellrechnungen werden mit tatsächlichen Meßergebnissen an Flammstrahlen verglichen, die unter definierten Bedingungen ein Abplatzen von Gestein hervorrufen. Die Versuche wurden mit Granitgestein aus Barre (in Vermont) und Westerly (Rhode Island) ausgeführt. Bei einem kleinen Propan/Sauerstoff-Überschall-Flammstrahl stimmt der berechnete Wärmeübergang üblicherweise innerhalb 20% mit experimentellen Werten überein. Die Eindringgeschwindigkeit bei den Bohrexperimenten, die ein weiteres Maß für die Wirksamkeit der Wärmeübertragung darstellt, ist hingegen um wenigstens einen Faktor 4 kleiner als erwartet. Diese Abweichung wird auf Einflüsse der Zweiphasen-Strömung und auf das Haften von Gesteinsteilchen an der abplatzenden Oberfläche zurückgeführt—beides Effekte, die nicht in dem Rechenmodell berücksichtigt werden.

ЧИСЛЕННОЕ МОДЕЛИРОВАНИЕ И ОПЫТНЫЕ ИССЛЕДОВАНИЯ СТРУЙНО-ФАКЕЛЬНОГО ТЕРМИЧЕСКОГО БУРЕНИЯ—2. ЭКСПЕРИМЕНТАЛЬНАЯ ПРОВЕРКА

Аннотация—Результаты расчетов по ранее разработанной модели сравниваются с натурными измерениями струйно-факельного расщепления породы в заданных экспериментальных условиях. Для испытаний выбраны гранитные породы из Барра, Вермонта и Уэстерли, Род-Айленд. Скорости теплопереноса, рассчитанные для мелкомасштабных пропано–кислородных сверхзвуковых струй пламени, обычно совпадали с тарировочными значениями с точностью до 20%; скорости же проникновения, полученные при экспериментах по добыче пород бурением и являющиеся другим критериям эффективности теплопереноса, значительно, по меньшей мере в 4 раза, ниже ожидаемых. Эффекты двухфазного течения и применение макрочастиц породы к отколоняющей поверхности, которые практически не учитываются в модели, вносят вклад в это расхождение.